Touring invariant-set boundaries of a two-vortex system using streamline control

Francis D. Lagor, Kayo Ide, and Derek A. Paley

Abstract— **This paper presents a path-planning control for an intermittently actuated oceanographic vehicle in a time-invariant flow field based on Lagrangian measurement data. The oceanographic focus is an idealized ocean-eddy system represented by two point vortices. We partition the model of the underlying flow into distinct invariant regions (in a co-rotating frame) and use this geometry to plan informative vehicle tours. Driving along the invariant-set boundaries increases the overall empirical observability of the flow field parameters. We validate the importance of invariant sets and set boundaries using the local unobservability index. To tour the boundaries of invariant sets, a novel control law drives the vehicle to a desired streamline value; another controller is based on the idea of inserting a virtual cylinder into the flow. Numerical experiments in the two-vortex system show the proposed Boundary-Touring Algorithm yields planned paths with high observability of the flow field parameters as compared to random drifter orbits.**

I. INTRODUCTION

Due to strong ocean-atmosphere coupling, improved understanding of the ocean through informative measurements may lead to better predictions in atmospheric climate variations on a wide range of time scales [1],[2]. Targeted observations are needed to cope with the ocean vastness and the corresponding sparsity of subsurface measurements. Although the Argo system (a global array of drifting platforms that capture temperature, current, and salinity data on vertical dives [2]) already provides subsurface measurements, these measurements are incredibly sparse—only 3,750 floats in 361,900,000 square kilometers of ocean [2],[3]. Observation sparsity motivates the need for sampling with long-endurance autonomous vehicles like underwater drifters (passive vehicles that operate at constant depth) and ocean gliders (steered vehicles that operate at variable depths) [4],[5],[6] in the design of the next global ocean observing system. While the benefits of underwater gliders for adaptive sampling have been established [4], there exists no comprehensive framework that takes advantage of ocean-current forecasts for autonomous and coordinated path planning of multiple, minimally actuated vehicles.

Francis D. Lagor is a graduate student in the Department of Aerospace Engineering, University of Maryland, College Park, MD 20742, USA. frank.lagor@gmail.com

Kayo Ide is an Associate Professor in the Department of Atmospheric and Oceanic Science, University of Maryland, College Park, MD 20742, USA. ide@umd.edu

Derek A. Paley is the Willis H. Young Jr. Associate Professor of Aerospace Engineering Education in the Department of Aerospace Engineering and the Institute for Systems Research, University of Maryland, College Park, MD 20742, USA. dpaley@umd.edu

This research is supported by the National Science Foundation under Award No. CMMI-1362837.

A path-planning framework for autonomous oceanographic vehicles should address transport barriers formed by coherent structures. Coherent structures in strong flows such as ocean eddies and gyres create (almost) invariant sets or entrained regions; a vehicle cannot leave the set without exerting control. There are many techniques for identifying coherent structures in flows [7]. For example, Lagrangian Coherent Structures (LCS) are calculated by finding the local maxima in a Finite Time Lyapunov Exponent (FTLE) field [8]. Another approach uses the stochastic Frobenius-Perron operator to examine the transition probabilities between spatially discretized cells [7]. Methods also exist for quantifying the uncertainty of such structures [9].

We examine the invariant sets created by an idealized point-vortex model, identified through the stable and unstable manifolds associated with saddle points in the flow. Two point vortices with the same-signed circulation strength co-rotate in relative equilbrium. When viewed in a co-rotating frame, the flow is time-invariant and six invariant sets are visible. The two-vortex system is the focus of this paper because it represents an idealized model of a pair of ocean eddies, and it is a natural extension of prior works on observability-based path planning in a uniform flow [10] and in the presence of a single, stationary point vortex [11].

Coherent structures are also important for long-endurance path planning [12], coverage and sampling [13], and understanding ocean transport processes in general [6]. Mallory *et al.* [14] used the geometric structure of a flow field partitioned along LCS boundaries along with a distributed hybrid-control strategy to maintain a desired distribution of sampling platforms across multiple invariant regions. Other prior works have examined energy [12] and time-optimality [15] of path planning for point-to-point navigation of a self-propelled vehicle using stochastic-optimization and level-set methods.

For extended-duration, ocean sampling missions, the assumption made in prior works that a vehicle is continuously self-propelled may not hold. For example, sampling platforms such as drifters passively advect with the flow. Salman *et al.* [16] investigated Lagrangian data assimilation using flow geometry to optimize drifter launch locations. In this paper, hypothetical vehicles use intermittent actuation to navigate like gliders, while spending most of the time drifting.

We propose sampling a two-vortex system along invariant set boundaries to improve the overall observability of the flow field parameters. We motivate this proposal using tools from nonlinear systems theory including the empirical observability Gramian. Krener and Ide [17] previously applied empirical observability to Lagrangian and Euler sensor deployment in a point-vortex flow. We extend their analysis of drifter launch location to consider the observability of complete orbits within invariant sets. Applying tools for theoretical hydrodynamics, including the Milne-Thomson circle theorem [18], we create guidance vector fields for vehicles to transition between adjacent boundaries by deforming flow streamlines around a virtual cylinder. We also create a novel control law for driving a vehicle to a desired streamline value. Using these control laws, we propose a boundary-sampling algorithm to generate vehicle tours through a two-vortex system with infrequent actuation.

The contributions of this paper are (1) a control law for guiding a vehicle to a specified streamline value of a time-invariant flow field; (2) a novel guidance strategy based on the deformation of flow streamlines around a virtual cylinder; and (3) a path-planning framework that guides a vehicle to actuate between boundaries of invariant sets for improved observability of a two-vortex system. Comparison of the overall empirical observability shows that a guided vehicle achieves higher empirical observability of the flow field parameters than any drifting vehicle (as determined through a Monte Carlo sampling of drifter deployment locations), without the need for launch optimization.

The outline of the paper is as follows. Section II provides background on invariant sets in a time-invariant flow field and introduces empirical observability analysis. Section III describes one control law for guiding an autonomous vehicle to a specified streamline value and another for guiding a vehicle around a saddle point location using a virtual cylinder. Section VI presents a numerical implementation of the path-planning algorithm, demonstrating the efficacy of this method by comparing a guided vehicle to drifting vehicles. Section V summarizes the paper and describes ongoing research.

II. INVARIANT SETS AND OBSERVABILITY

A. Invariant sets in a two-vortex flow

For two-dimensional incompressible flow, the flow-field velocities v_x and v_y are conveniently expressed in terms of the stream function $\psi(x, y, t)$ by [19]

$$v_x = \frac{\partial\psi}{\partial y}(x, y, t) \quad \text{and} \quad v_y = -\frac{\partial\psi}{\partial x}(x, y, t). \tag{1}$$

If the flow is time-invariant, then $\psi = \psi(x, y)$. We make the correspondence $z = x + iy$ between the two-dimensional (x, y) plane and the complex plane for compactness, so that $\psi = \psi(z, \bar{z})$. (The overbar denotes conjugation.)

A point vortex is a mathematical construct in potential flow theory in which all vorticity (two times the angular velocity) of the surrounding fluid is concentrated in a singularity at its center [19]. In this way, the flow field is irrotational (free of vorticity) everywhere except at the center of the point vortex. The irrotational flow field permits convenient mathematical manipulation due to its linearity and the existence of a potential function for the flow velocity. For two point vortices located at z_1, z_2 with circulation strengths γ_1, γ_2, the flow field is generated by the stream function [19]

$$\psi(z, \bar{z}) = -\frac{1}{2\pi}\left(\gamma_1 \log|z - z_1| + \gamma_2 \log|z - z_2|\right). \tag{2}$$

A vehicle that drifts passively with the flow has dynamics described by [19]

$$\dot{z} = \dot{x} + i\dot{y} = \frac{\partial\psi}{\partial y} - i\frac{\partial\psi}{\partial x} = -2i\frac{\partial\psi}{\partial\bar{z}}, \tag{3}$$

where we use the definition of the complex partial-derivative operator

$$\frac{\partial}{\partial\bar{z}} = \frac{1}{2}\left(\frac{\partial}{\partial x} + i\frac{\partial}{\partial y}\right). \tag{4}$$

Since two vortices with same-signed circulation strength co-rotate at an angular rate of $\omega = \frac{\gamma_1+\gamma_2}{2\pi|z_1-z_2|^2}$ [19], it is often advantageous to consider the dynamics in a co-rotating frame, under the change of variables $z = \xi e^{i(\omega t+\phi)} + z_{cv}$, where ϕ is an initial phase angle and z_{cv} is the center of vorticity (center of the rotating frame). The dynamics of a drifting vehicle become

$$\dot{\xi} = -2i\frac{\partial\psi}{\partial\bar{\xi}} - i\omega\xi = -2i\frac{\partial\psi_R}{\partial\bar{\xi}}, \tag{5}$$

where the co-rotating frame stream function is

$$\psi_R = \psi + \frac{\omega}{2}|\xi|^2. \tag{6}$$

The streamlines associated with ψ_R are shown in Fig. 1(a), along with the fixed points of the flow. We numerically implement a Rankine vortex, in which the flow speed is scaled linearly down to zero close to the center to handle the singularity there.

In the study of transport in dynamical systems (see, e.g., [20]), it is convenient to enumerate naturally occurring invariant regions of the differentiable manifold on which the dynamical system evolves. More precisely, let $\mathcal{M}$ denote the differentiable manifold in the phase space of the system dynamics. Let *region* $\mathcal{R}_i$, $i = 1, \ldots, N_r$, be a connected subset of $\mathcal{M}$ with boundaries consisting of the boundaries of $\mathcal{M}$ (possibly at infinity) and/or segments of stable and unstable manifolds of the system dynamics [20]. $\mathcal{M}$ is then the union of the invariant regions [20], i.e., $\mathcal{M} = \bigcup_{i=1}^{N_r} \mathcal{R}_i$. A key hypothesis of this paper is that driving a vehicle along the boundaries of multiple invariant regions provides valuable information for flow field estimation that may be unobtainable by drifting trajectories that are confined to individual regions of the flow.

Fig. 1(c) and 1(d) show examples of invariant regions induced by two co-rotating vortices of equal and unequal strength, respectively. These figures were generated by the following procedure for region delineation based on flow-field geometry. First, identify fixed points in the flow field. For the two-vortex problem, fixed point locations are determined analytically (see, e.g., [19]). In the case of flow fields for which there is an associated stream function, the fixed points are either centers or saddles. The second step is to determine the stable and unstable manifolds of the saddle

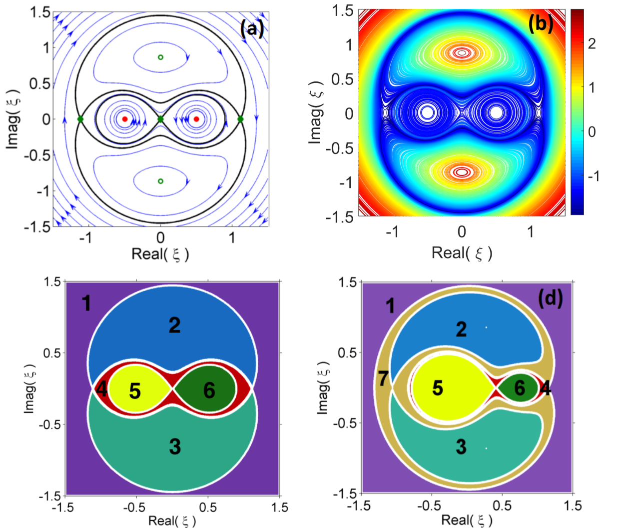

Fig. 1: (a) The two-vortex system in a co-rotating frame. Blue lines are streamlines of the flow and black lines are separatices. Red markers indicate the vortex singularities, green circles are centers, and green diamonds are saddle points. (b) Log of the unobservability index for orbits in the two-vortex system. (c)-(d) Invariant regions of the flow field around a pair of co-rotating vortices with equal strength and unequal strength, respectively.

fixed points. When a stream function is available, the stream-function values of the stable and unstable manifolds are the stream-function values of the corresponding saddle points. Other methods exist for calculating the stable and unstable manifolds of a hyperbolic trajectory [21], however, these are beyond the scope of this paper.

B. Empirical observability

In linear systems theory, if the observability Gramian $W_o(t_0, t_1)$ is nonsingular on the time interval $[t_0, t_1]$, then one can infer the initial state of the system from the output over this interval [17]. The observability Gramian for linear systems provides a boolean answer to the question of observability. For the nonlinear system

$$\dot{X} = f(t, X) \quad \text{with} \quad Y = h(t, X), \tag{7}$$

where $X \in \mathbb{R}^n$ and $Y \in \mathbb{R}^m$, Krener and Ide [17] construct an *empirical observability Gramian* $W_o(t_0, t_1) \in \mathbb{R}^{nxn}$ based on output correlations that result from perturbing the initial state of the system. Empirical observability is a local, linear approximation to nonlinear observability under perturbation of the n parameters or initial state entries that need to be inferred. $W_o(t_0, t_1)$ is given by its (i, j)th entries [11],[17]

$$\begin{aligned} W_o(i,j) = \frac{1}{4\epsilon_i\epsilon_j} \int_{t_0}^{t_1} & \left[Y^{+i}(\tau) - Y^{-i}(\tau)\right]^T \times \\ & \left[Y^{+j}(\tau) - Y^{-j}(\tau)\right] d\tau, \quad \text{for } i, j = 1, \ldots, N, \end{aligned} \tag{8}$$

where $Y^{\pm i}(\tau)$ is the output at time τ that results from initial condition $X^{\pm i}(t_0) = Z(t_0) \pm \epsilon_i e_i$, which has been perturbed along the direction of the e_i unit vector. The reciprocal of the smallest singular value of $W_o(t_0, t_1)$ provides a measure of how difficult it is to infer the initial state by observing the output on the interval $[t_0, t_1]$ [17]. This measure is called the (local) unobservability index $\nu \triangleq 1/\sigma_{\min}$.

We utilize the unobservability index ν to quantify the informativeness of various orbits in the two-vortex system by letting

$$X = (\mathrm{Re}(z), \mathrm{Im}(z), \mathrm{Re}(z_1), \mathrm{Im}(z_1), \gamma_1, \mathrm{Re}(z_2), \mathrm{Im}(z_2), \gamma_2)^T,$$

where z_i and γ_i are the inertial location and circulation strength of vortex $i = 1, 2$. The unobservability index is calculated by considering perturbations of flow field parameters z_1, γ_1, z_2, and γ_2. Lagrangian measurements of the vehicle positions are taken, i.e., $Y = [\mathrm{Re}(z), \mathrm{Im}(z)]^T$.

Orbits are of interest, both for drifting vehicles on extended deployments and for vehicles that actuate infrequently. Krener and Ide [17] examined the unobservability index over one period of the two-vortex system to assess launch locations for Lagrangian drifters. We have extended this analysis to closed orbits in the following manner. We first performed a grid-based unobservability analysis similar to [17], with a longer time horizon that ensures all of the drifters in the domain achieve a full orbit. (The integration time was 24π, permitting approximately one period for the longest-duration orbit and more than one period for other orbits.) For each orbit considered, we assigned to the curve the average value of the unobservability index from the grid-based analysis. The grid-based analysis provides an estimate of the best launch location, whereas the orbit averages provide estimates from which dependence on the initial conditions has been removed. Fig. 1(b) presents the results of this calculation for 1000 orbits from random initial conditions selected from a uniform distribution over the domain. The least informative orbits in the two-vortex system occur near the center fixed points in regions 2 and 3. Fig. 1(b) shows that the most informative orbits occur very close to the separating boundaries between invariant sets. This observation motivates the sampling algorithm in Section IV.

III. NAVIGATION OF SET BOUNDARIES

A. Driving to a desired streamline value

To plan a vehicle's path within a flow field, consider an actuated vehicle that moves according to the sum of the drift vector field (generated by a time-invariant stream function) and a control vector field, i.e.,

$$\dot{z} = -2i \frac{\partial \psi}{\partial \bar{z}}\bigg|_z + u. \tag{9}$$

(For the co-rotating frame, replace ψ with ψ_R, z with ξ, and u with u_R.) These dynamics are intended only to generate trajectories that will be tracked by onboard, lower-level controllers. Vehicle-specific dynamic constraints (e.g., limitations on speed or turning control) are beyond the scope of this paper. We include a saturation $\mathrm{sat}(u; u_{\max})$ as a placeholder for such physical limitations.

Suppose we seek to drive the vehicle (i.e., design a path) to a desired stream function value ψ_R^{des} in the co-rotating frame. The following proposition provides a control u_R that asymptotically drives ψ_R to ψ_R^{des}, provided $\frac{\partial \psi_R}{\partial \bar{\xi}} \neq 0$, which we ensure later.

Proposition 1: For a vehicle with dynamics (9) in a flow given by stream function ψ_R, the control law

$$u_R = -K\left(\psi_R - \psi_R^{\text{des}}\right) \frac{\frac{\partial \psi_R}{\partial \bar{\xi}}}{\left|\frac{\partial \psi_R}{\partial \bar{\xi}}\right|^2} \tag{10}$$

drives the vehicle to the streamline corresponding to ψ_R^{des}, provided that $\frac{\partial \psi_R}{\partial \bar{\xi}} \neq 0$.

Proof: Let $V \triangleq \frac{1}{2}(\psi_R - \psi_R^{\text{des}})^2$ be a candidate Lyapunov function. Along trajectories of the closed-loop dynamics[1],

$$\dot{V} = \left(\psi_R - \psi_R^{des}\right) \left\langle 2\frac{\partial \psi_R}{\partial \bar{\xi}}, \dot{\xi} \right\rangle = -2K\left(\psi_R - \psi_R^{des}\right)^2 \leq 0.$$

Invoking the invariance principle [22] shows that all trajectories converge to the largest invariant set for which $\dot{V} = 0$. The invariance condition $\psi_R - \psi_R^{\text{des}} \equiv 0$ implies that $\psi_R = \psi_R^{\text{des}}$ in this set. ∎

Note that for a planar flow defined by a stream function, only center and saddle fixed points are possible. A center fixed point is either a local minimum or maximum of ψ_R. If the vehicle begins near (but not on) a center and ψ_R^{des} represents a streamline away from the vehicle and the center, then the coefficient $-K(\psi_R - \psi_R^{\text{des}})/|\frac{\partial \psi_R}{\partial \bar{\xi}}|^2$ of the gradient $\frac{\partial \psi_R}{\partial \bar{\xi}}$ is negative for a local maximum and positive for a local minimum; in either case, u_R always drives the vehicle outward from the center. Saddle points are avoided by introducing virtual cylinders in Section IV that prevent vehicle intrusion.

The control effort under (10) is zero when $\psi_R = \psi_R^{\text{des}}$, which implies the vehicle acts as a drifter when the desired streamline is reached. All calculations in this paper are performed in the inertial frame, because observability calculations require parameter perturbations that affect the rotation rate ω. The frame transformation is $u(z) = u_R(\xi(z))\frac{\partial \bar{\xi}}{\partial \bar{z}}$, and control law (10) described in the inertial frame using (6) is

$$u = -K\Big(\psi(z) - \frac{\omega}{2}|z - z_{cv}|^2 - \psi_R^{\text{des}}\Big) \frac{\frac{\partial \psi}{\partial \bar{z}} + \frac{\omega}{2}(z - z_{cv})}{|\frac{\partial \psi}{\partial \bar{z}} + \frac{\omega}{2}(z - z_{cv})|^2}. \tag{11}$$

B. Virtual cylinders for saddle avoidance

If the flow field is described using a complex potential $w(z)$, then according to the Milne-Thomson circle theorem [18], the complex potential that would result after placing a cylinder of radius a at the origin is

$$W(z) = w(z) + \overline{w}\left(\frac{a^2}{z}\right). \tag{12}$$

($\overline{w}\left(\frac{a^2}{z}\right)$ is found by forming the complex conjugate $\overline{w(z)}$ and subsequently replacing $\overline{z}$ everywhere with $\frac{a^2}{z}$ [18].)

Proposition 2 (Circle theorem using the stream function): Given a flow described by stream function $\psi(z)$, the stream function that results after placing a cylinder of radius a in the flow at the origin is

$$\Psi = \psi(z) - \overline{\psi}\left(\frac{a^2}{z}\right). \tag{13}$$

Proof: $w(z)$ may be expressed as $w(z) = \phi(z, \overline{z}) + i\psi(z, \overline{z})$, where ψ is the streamfunction. The velocity potential and stream function are real-valued, but they may be expressed as functions of z and $\overline{z}$, i.e.,

$$\Phi + i\Psi = (\phi(z,\overline{z}) + i\psi(z,\overline{z})) + \left(\overline{\phi}\left(\frac{a^2}{z}, \frac{a^2}{\overline{z}}\right) - i\overline{\psi}\left(\frac{a^2}{z}, \frac{a^2}{\overline{z}}\right)\right).$$

Suppressing conjugate arguments[2] implies (13). ∎

Corollary 1 (Circle theorem for an off-origin cylinder): Given a flow described by stream function $\psi(z)$, the stream function that results after placing a cylinder of radius a at location c in the flow field is

$$\Psi(z) = \psi(z) - \overline{\psi}\left(\frac{a^2}{z - c} + \overline{c}\right). \tag{14}$$

Proof: Consider the change of coordinates, $\hat{z} = z - c$. Define $\psi_c(\hat{z})$ to be the stream function in terms of $\hat{z}$, i.e., $\psi_c(\hat{z}) = \psi(\hat{z} + c)$. Applying the circle theorem to ψ_c yields

$$\Psi_c(\hat{z}) = \psi_c(\hat{z}) - \overline{\psi}_c\left(\frac{a^2}{\hat{z}}\right) = \psi(\hat{z} + c) - \overline{\psi}\left(\frac{a^2}{\hat{z}} + \overline{c}\right).$$

Returning to z coordinates with $\Psi(z) = \Psi_c(z - c)$ yields (14). ∎

Fig. 2(a) shows how the virtual streamlines are deformed by inserting a virtual cylinder into a two-vortex flow at ξ_c. Note that for this cylinder size and location, the invariant regions of the flow are preserved, i.e., a vehicle following these guidance streamlines would not switch sets. To allow for additional flexibility in streamline deformation, we include circulation κ so that the stream function becomes

$$\Psi_R(\xi) = \psi_R(\xi) - \overline{\psi}_R\left(\frac{a^2}{\xi - \xi_c} + \overline{\xi_c}\right) + \kappa \log\frac{|\xi - \xi_c|}{a}. \tag{15}$$

The inclusion of circulation κ is equivalent to spinning the cylinder at a rate of $\frac{\kappa}{2\pi a^2}$ [18]. Fig. 2(b) and 2(c) show the guidance streamlines now cross boundaries near the cylinder.

When the vehicle is sufficiently close to the cylinder (i.e., within activation radius $r_a = 2a$), the cylinder control is engaged. The cylinder-control input to the vehicle is the combination of the flow associated with the guidance stream function Ψ_R minus the actual flow, i.e.,

$$u_R = -2i\left(\frac{\partial \Psi_R}{\partial \bar{\xi}} - \frac{\partial \psi_R}{\partial \bar{\xi}}\right). \tag{16}$$

Fig. 2(d) shows the parameters associated with the cylinder-control law used to navigate saddles. The locations of the region boundary intersections with the activation area are maintained for each cylinder. The vehicle avoids flow stagnation points on the surface of the cylinder and turns right or left by choosing the sign of κ accordingly. (Positive (resp. negative) κ corresponds to counterclockwise (resp.

[1] $\langle a, b\rangle = \text{Re}(\overline{a}b)$ denotes the inner product of complex scalars a and b.

[2] We suppress conjugate arguments for notational simplicity. $w(z)$ is analytic and does not depend on $\overline{z}$, but ψ can depend on z and $\overline{z}$.

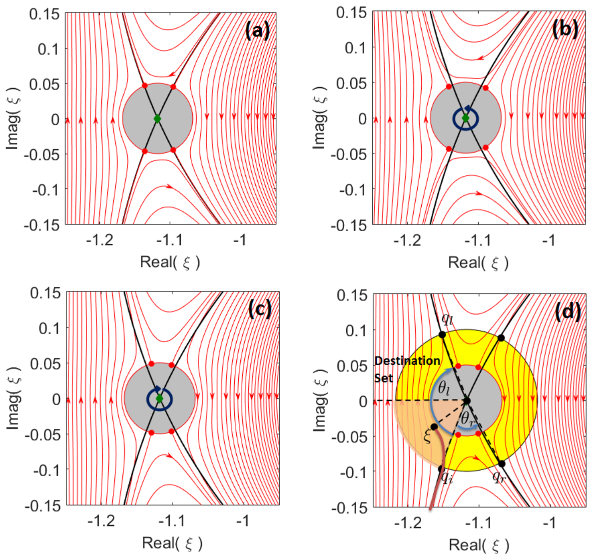

Fig. 2: (a) Guidance streamlines after addition of virtual cylinder; (b)-(c) guidance streamlines for a virtual cylinder with counter-clockwise and clockwise circulation, respectively. (d) Geometry of the cylinder-control law at a saddle point. Black lines represent the separating boundaries in the actual flow field. Red circles represent stagnation points.

clockwise) circulation, which generates a left (resp. right) turn.) As shown in Fig. 2(d), the vehicle calculates the angle between q_i and q_f, which are the initial and final intersection points used in the cylinder control. The q_f point is selected to be either q_l or q_r, for a left or right turn. The cylinder control is active until the angle between q_i and the vehicle exceeds one half of the angle between q_i and q_f, ensuring the vehicle has steered away from the saddle.

IV. Boundary-Touring Algorithm

This section presents a numerical algorithm for touring the invariant set boundaries of a known two-vortex system, with an idealized sampling vehicle. The vehicle is modeled as a Lagrangian sensor, i.e., it advects with the flow, collecting measurements of its own position subject to infrequent actuation. The algorithm drives the vehicle around a *tour*, which is a planned path along region boundaries.

The Boundary-Touring Algorithm (BTA) assumes the vehicle has a region map based on the partitioning described in Section II. The region map yields a connected region graph that is useful for tour design. The undirected region graph $G = (V, E)$ is constructed with the region labels as the vertices, so that the vertex set is $V = \{1, \ldots, M\}$ and the edge set E consists of all separating boundaries. Only adjacent regions produce edges; two regions are adjacent if they share a boundary, excluding pairs that share only a point. The values of the stream function $\psi_{i,j}$ between regions i,j are stored as a symmetric adjacency matrix A, known to the vehicle, where $a_{i,j} = \psi_{i,j}$ if vertices i,j have an edge in E and $a_{i,j} = 0$ otherwise. Each vehicle also maintains a list of predetermined virtual-cylinder locations (in the co-rotating frame) and of locations of boundary intersection

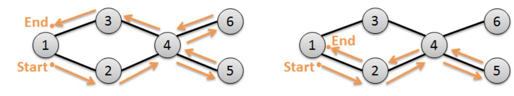

(a) (1, 2, 4, 5, 4, 6, 4, 3, 1) (b) (1, 2, 4, 5, 4, 2, 1)

Fig. 3: Region graphs and tours for the two-vortex system.

TABLE I: Boundary-Touring Algorithm

1 Identify invariant sets (regions) $D = \{\mathcal{R}_1, \ldots, \mathcal{R}_M\}$ and construct region graph $G = (V, E, A)$.
2 Get current region: k = getRegion(z, D).
3 Generate tour $\mathcal{T}(G) \leftarrow (\mathcal{R}_k, \mathcal{R}_j, \ldots, \mathcal{R}_k)$ to visit a desired subset of vertices, starting at k.
4 Get next region n in tour $\mathcal{T}$.
5 **while** 1 **do**
  Converge to streamline
6   Set $\psi^{\text{des}} = \psi_{k,n}$ until encountering a cylinder activation area.
  Cylinder interaction
7   Set $q_i = q_{k,j}$ to be the closest intersection point of the separating boundary and activation area;
8   Select $q_f = q_{k,n}$ to visit next region n if available, else turn to visit another cylinder;
9   Select sign of circulation κ based on turn direction;
10   **while** $|\angle(q_i, \xi)| < \frac{1}{2}|\angle(q_i, q_f)|$ **do**
11     $u_R = -2i\left(\frac{\partial \bar{\Psi}_R}{\partial \xi} - \frac{\partial \psi_R}{\partial \xi}\right)$.
12   $u_R = 0$.
13   Get current region: k = getRegion(z, D).
14   **if** k = n **then**
15   Get next region n in tour $\mathcal{T}$.
16   **Repeat**: Go to line 5.

points for each cylinder's activation area (see Fig. 2(d)). For an estimated flow, these locations are based on the best-guess parameter values and may be refined iteratively.

A vehicle tour is a cycle in the graph (i.e., a path that begins and ends at the same vertex) that passes through a subset of the vertices. A vehicle is able to query its current region using its location and the region map. A vehicle visits a region when it briefly enters it during boundary switching near a saddle point. Fig. 3(a) and 3(b) show the region graph for a two-vortex system and two possible sampling tours. The tour in Fig. 3(a) visits all of the boundaries, whereas the tour in Fig. 3(b) visits only a subset of the boundaries. For equal-strength vortices, $\gamma_1 = \gamma_2$, the tour in Fig. 3(b) may be sufficient for high observability due to symmetries in the flow field. Determining a sufficient tour for observability purposes is the subject of ongoing work.

Table I presents the overall approach to boundary touring. There are two main subroutines: (1) streamline convergence and (2) cylinder interaction. As long as sampling is required, the vehicle cycles through tour $\mathcal{T}$ as follows. First it converges to the streamline associated with a boundary. When a vehicle encounters a cylinder activation area, it uses the cylinder control to avoid a saddle point. Fig. 4(a) illustrates the BTA for the two-vortex system from an initial location in region 1, for the tour $\mathcal{T} = (1, 2, 4, 5, 4, 2, 1)$. Fig. 4(b) presents the control cost for this portion of the tour relative to the maximum flow speed the vehicle may encounter in the domain. (The maximum is well-defined due to the use of Rankine vortices.) Note infrequent actuation occurs and $|u|$ is negligible (defined here to be $|u| < 0.005 \max(|v_x + iv_y|)$)

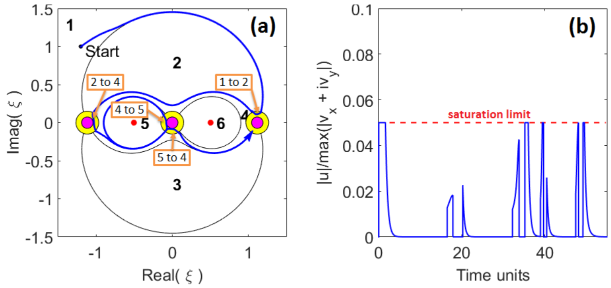

Fig. 4: (a) A vehicle performing the BTA for tour (1, 2, 4, 5, 4, 2, 1). Yellow circles indicate cylinder activation areas, and magenta circles are virtual cylinders. (b) The associated control cost for this portion of the simulation.

TABLE II: Unobservability indices for $W_o(0, 24\pi)$. (Note: lower is better.)

	N	Minimum	Mean	Maximum
Gridded analysis	10000	1.95×10^{-4}	18.62	4.86×10^{3}
Orbit analysis	1000	1.26×10^{-2}	17.07	564.67
Tour (1,2,4,5,4,6,4,3,1)	100	1.57×10^{-4}	0.0045	0.0390
Tour (1,2,4,5,4,2,1)	100	8.46×10^{-5}	0.0043	0.0388

for large portions of the tour. For example, the vehicle in Fig. 4(a) spent 79.1% of its time drifting.

To assess the performance of the BTA, we compare a controlled vehicle to a drifting vehicle by calculating the empirical observability along each trajectory. The empirical observability Gramian [17] is defined for system (7) along candidate trajectories. For a controlled trajectory, we calculate $W_o(0, 24\pi)$ by taking $u(t)$ (found in simulation of the vehicle tour) as a known function of time. The controlled vehicle tour in Fig. 4(a) yields an unobservability index of 1.42×10^{-2} (high observability) for the same time horizon used for the drifter orbit evaluation of Fig. 1(b).

A comparison of the grid-based observability analysis, the orbit-averaged analysis, and the BTA for two candidate tours is shown in Table II. For each tour, 100 random (uniformly distributed) initial conditions in region 1 were selected. Both tours produced trajectories that are more observable than the best drifter trajectories. The mean controlled values were also more observable than the mean drifting values, which implies the BTA can yield trajectories with high observability, without launch optimization and with infrequent actuation. The BTA is also amenable to online re-planning for estimated flow fields, whereas drifter launch optimization is not.

V. CONCLUSIONS AND ONGOING WORK

This work describes a principled approach for touring invariant set boundaries of a two-vortex flow field using infrequent actuation. The transition of the vehicle between boundaries is accomplished using a novel streamline control law and the inclusion of a virtual cylinder that creates guidance vectors from virtual streamlines. The cylinder appears in the flow in front of the vehicle at locations of saddle points. In a numerical experiment, the boundary sampling algorithm achieves high empirical observability of the flow field parameters without the need for launch optimization. In ongoing work, we aim to extend this research to understand the relative benefits of tours that do not visit all boundaries and to understand the roles that multiple vehicles may play in boundary coverage.

VI. ACKNOWLEDGMENTS

The authors acknowledge valuable discussions with Storm Weiner (supported by the NSF TREND REU program).

REFERENCES

[1] L.D. Talley, G.L. Pickard, W.J. Emery, and J.H. Swift, Descriptive physical oceanography: An introduction, Academic Press, Elsevier, London, 6th edition, 2011.
[2] M. Belbeoch, "Argo: Part of the integrated global observation strategy," http://www.argo.ucsd.edu/, Accessed: 2014-12-15.
[3] B. W. Eakins and G. F. Sharman, "Volumes of the world's oceans from ETOPO1," http://www.ngdc.noaa.gov/mgg/global/etopo1_ocean_volumes.html, Accessed: 2014-12-21.
[4] B. Mourre and A. Alvarez, "Benefit assessment of glider adaptive sampling in the Ligurian Sea," Deep Sea Res. Part I Ocean. Res. Papers, vol. 68, pp. 68–78, 2012.
[5] D. A. Paley, F. Zhang, and N. E. Leonard, "Cooperative control for ocean sampling: The Glider Coordinated Control System," IEEE Trans. Control Sys. Tech., , no. 1063-6536, pp. 1–10, 2008.
[6] R. N. Smith, M. Schwager, S. L. Smith, B. H. Jones, D. Rus, and G. S. Sukhatme, "Persistent ocean monitoring with underwater gliders: Adapting sampling resolution," J. Field Robotics, vol. 28, no. 5, pp. 714–741, 2011.
[7] L. Billings and I. B Schwartz, "Identifying almost invariant sets in stochastic dynamical systems.," Chaos, vol. 18, no. 2, 2008.
[8] S. C Shadden, F. Lekien, J. D. Paduan, F. P. Chavez, and J. E. Marsden, "The correlation between surface drifters and coherent structures based on high-frequency radar data in Monterey Bay," Deep Sea Res. Part II Top. Stud. Oceanogr., vol. 56, no. 35, pp. 161–172, 2009.
[9] S. Ravela, "Quantifying uncertainty for coherent structures," Procedia Comp. Sci., vol. 9, pp. 1187–1196, 2012.
[10] B. T. Hinson, M. K. Binder, and K. A. Morgansen, "Path planning to optimize observability in a planar uniform flow field," in Amer. Control Conf., Washington, DC, 2013, number 1, pp. 1394–1401.
[11] L. DeVries, S. J. Majumdar, and D. A. Paley, "Observability-based optimization of coordinated sampling trajectories for recursive estimation of a strong, spatially varying flowfield," J. Intell. Robot. Syst., vol. 70, no. 1-4, pp. 527–544, 2012.
[12] D. N. Subramani, T. Lolla, P. J. Haley Jr., and P. F. J. Lermusiaux, "A stochastic optimization method for energy-based path planning," in Dyn. Data-driven Environ. Syst. Sci. Conf., 2014.
[13] E. Forgoston, L. Billings, P. Yecko, and I. B Schwartz, "Set-based corral control in stochastic dynamical systems: making almost invariant sets more invariant.," Chaos, vol. 21, no. 1, 2011.
[14] K. Mallory, M. A. Hsieh, E. Forgoston, and I. B. Schwartz, "Distributed allocation of mobile sensing swarms in gyre flows," Nonlinear Process. Geophys., vol. 20, pp. 657–668, 2013.
[15] T. Lolla, M. P. Ueckermann, K. Yigit, P. J. Haley Jr., and P. F. J. Lermusiaux, "Path planning in time dependent flow fields using level set methods," in IEEE Int. Conf. Robotics and Automation (ICRA), 2012, pp. 166–173.
[16] H. Salman, K. Ide, and C. K. R. T. Jones, "Using flow geometry for drifter deployment in Lagrangian data assimilation," Tellus A, vol. 60, no. 2, pp. 321–335, 2008.
[17] A. J. Krener and K. Ide, "Measures of unobservability," 48th IEEE Conf. Decision Control, pp. 6401–6406, 2009.
[18] L. M. Milne-Thomson, Theoretical hydrodynamics, Dover, New York, 5th edition, 1968.
[19] P. K. Newton, The N-vortex problem: Analytical techniques, Springer, New York, 2001.
[20] Stephen Wiggins, Chaotic transport in dynamical systems, Springer-Verlag, New York, 1992.
[21] A. M. Mancho, D. Small, S. Wiggins, and K. Ide, "Computation of stable and unstable manifolds of hyperbolic trajectories in two-dimensional, aperiodically time-dependent vector fields," Phys. D Nonlinear Phenom., vol. 182, pp. 188–222, 2003.
[22] H. Khalil, Nonlinear systems, Prentice Hall, Upper Saddle River N.J., 3rd edition, 2002.